

PNP-U3D: Plug-and-Play 3D Framework Bridging Autoregression and Diffusion for Unified Understanding and Generation

Yongwei Chen^{1†}, Tianyi Wei^{1†}, Yushi Lan², Zhaoyang Lyu³, Shangchen Zhou¹, Xudong Xu³, Xingang Pan^{1*}

¹*S-Lab, Nanyang Technological University, 50 Nanyang Avenue, Singapore, 639798, Singapore, Singapore.

²Department of Engineering Science, University of Oxford, Parks Road, Oxford, OX1 3PJ, Oxfordshire, United Kingdom.

³Shanghai Artificial Intelligence Laboratory, Longhua, Shanghai, 200032, Shanghai, China.

*Corresponding author(s). E-mail(s): xingang.pan@ntu.edu.sg;
Contributing authors: yongwei001@ntu.edu.sg; tianyi.wei@ntu.edu.sg;
yushi@robots.ox.ac.uk; lvzhaoyang@pjlab.org.cn; sczhou@ntu.edu.sg;
xuxudong@pjlab.org.cn;

†These authors contributed equally to this work.

Abstract

The rapid progress of large multimodal models has inspired efforts toward unified frameworks that couple understanding and generation. While such paradigms have shown remarkable success in 2D, extending them to 3D remains largely underexplored. Existing attempts to unify 3D tasks under a single autoregressive (AR) paradigm lead to significant performance degradation due to forced signal quantization and prohibitive training cost. Our key insight is that the essential challenge lies not in enforcing a unified autoregressive paradigm, but in enabling effective information interaction between generation and understanding while minimally compromising their inherent capabilities and leveraging pretrained models to reduce training cost. Guided by this perspective, we present the first unified framework for 3D understanding and generation that combines autoregression with diffusion. Specifically, we adopt an autoregressive next-token prediction paradigm for 3D understanding, and a continuous diffusion paradigm for 3D generation. A lightweight transformer bridges the feature space of large language models and the conditional space of 3D diffusion models, enabling effective cross-modal information exchange while preserving the priors learned by standalone models. Extensive experiments demonstrate that our framework achieves state-of-the-art performance across diverse 3D understanding and generation benchmarks, while also excelling in 3D editing tasks. These results highlight the potential of unified AR+diffusion models as a promising direction for building more general-purpose 3D intelligence. Project page: <https://cyw-3d.github.io/PnP-U3D/>.

Keywords: 3D Understanding, 3D Generation, 3D Editing, Unified Model

1 Introduction

Recently, with the advent of GPT-4o [1] and its remarkable performance in 2D understanding and generation, the research community has made substantial progress in exploring unified 2D models [2–5], particularly in terms of data representation, model architectures, and training strategies. Such unification promises synergistic benefits: a single model can share representations between perception and synthesis, improve data efficiency, and enable new capabilities like multimodal reasoning. In parallel, both 3D understanding [6] and 3D generation [7–10] have respectively reached new heights. Nevertheless, unified models that jointly address 3D understanding and generation remain largely underexplored.

Inspired by recent successes of unified understanding-generation models in 2D, we aim to develop a unified framework for 3D understanding and generation, taking a pivotal step toward more capable and versatile 3D models. The central challenge is to bridge the asymmetry between large-scale language priors for understanding and the comparatively small 3D datasets for generation, enabling information exchange while preserving the strengths of both. ShapeLLM-Omni [11] recently pioneered a purely autoregressive (AR) framework to unify 3D understanding and generation. While this approach aligns training objectives under a single paradigm, it requires discretizing continuous 3D signals into tokens, which inevitably degrades performance and prevents effective use of pretrained LLM priors. Consequently, it suffers from information loss due to quantization, high training costs, and limited compatibility with existing models and pipelines.

In this work, we present, to our knowledge, the first unified 3D AR+diffusion framework that couples autoregression for understanding with diffusion for generation. The framework is lightweight, broadly compatible, and better preserves priors learned by specialized understanding and generation models. This design is particularly suitable for 3D, where data is far scarcer than in 2D images-text corpora. Our insight is that the key to this task lies not in enforcing a unified autoregressive paradigm but in *enabling efficient interaction between 3D understanding and generation while preserving their respective strengths and leveraging pretrained models*.

Our framework employs an autoregressive next-token prediction paradigm for the understanding, while the generation follows the continuous diffusion paradigm. Concretely, we append a fixed-length set of learnable query tokens to the user input, which elicit relevant knowledge and produce informative representations via the language model [12]. A lightweight transformer then projects these representations into the original conditional embedding space of a 3D diffusion model, serving as an adaptation module between the LLM feature space and the diffusion generator. This preserves the native AR and diffusion paradigms while enabling effective information exchange without degrading 3D signal fidelity. The same mechanism naturally extends to 3D editing: providing 3D inputs to the understanding module yields guidance signals that pilot generation according to user instructions. The framework is computationally efficient and integrating seamlessly with diverse pretrained 3D understanding and generation models.

Extensive quantitative and qualitative experiments, along with ablations, demonstrate strong performance on both 3D understanding and generation tasks and validate the effectiveness of the lightweight design. We also showcase promising results on 3D editing.

2 Related Work

3D Generative Models. Previous methods for 3D generation can be categorized into two families. The first approach leverages 2D diffusion priors [13–16] to generate 3D objects via an optimization-based pipeline [17–19]. However, these methods are computationally intensive and prone to oversaturation artifacts. In contrary, native 3D generative models [7, 8, 20–28] have recently emerged for high-quality, efficient, and scalable 3D generation. Most follow a two-stage pipeline: (i) learning a VAE [29, 30] that encodes 3D objects into a latent space [7, 31–33], and (ii) training a latent generative model on these latents [30, 34, 35]. Owing to their scalability, such native 3D generative models are already being explored for commercial applications [9, 36, 37]. However, despite this progress, their editing capabilities—especially under a unified understanding-and-generation paradigm [1]—remain underexplored. What is more, our method demonstrates

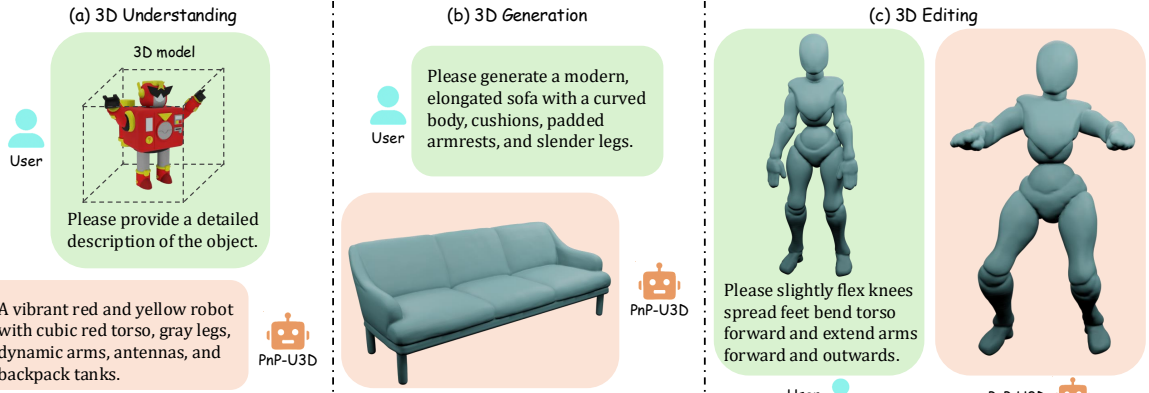


Fig. 1: PnP-U3D: the first unified 3D AR+Diffusion framework, enabling 3D understanding, generation, and editing.

remarkable 3D generation capability, as shown in Figure 2.

3D Understanding Models. The rapid progress of large language models (LLMs) [38–42] has catalyzed multimodal research that grounds language in 3D signals. Recent 3D understanding models integrate point clouds, depths, and multi-view images to support tasks such as 3D captioning, question answering, grounding, and reasoning about geometry and semantics [6, 43–51]. Despite steady gains, these systems are designed for understanding and therefore do not natively support 3D generation or editing.

Unified Understanding and Generation Models. Pioneered in 2D by GPT-4o [1], unified models have driven advances in data curation [2, 3, 52], representation design [53–55], architectures [2, 56, 57], and training strategies [3, 58, 59]. Representative paradigms include purely autoregressive (AR) [60–62], AR+diffusion [2, 63], and AR+visual-autoregression (VAR) [64]. On the 3D side, recently ShapeLLM-Omni [11] proposed a purely AR pipeline; while objective-unified, it suffers from quantization-induced information loss, high training cost, and limited compatibility with existing 3D generative backbones. In this work, we introduce (to our knowledge) the first unified 3D AR+Diffusion framework: *autoregression for understanding, diffusion for generation*. The design is lightweight, highly compatible, and preserves strong priors from standalone understanding and generation models—properties especially valuable in the data-scarce 3D regime.

3 Proposed Method

In this section, we present PnP-U3D, a lightweight framework for unified 3D understanding and generation that integrates the pretrained priors from an autoregressive vision-language model (VLM) and a 3D diffusion model. More formally, we aim to approximate the joint distribution $p_\theta(x, t)$ over 3D shapes x and text t , enabling inference over its conditionals for understanding $p_\theta(t | x)$, generation $p_\theta(x | t)$, and editing $p_\theta(x_{\text{edit}} | x_{\text{input}}, t)$. Practically, the system accepts text prompts and/or 3D shapes and produces semantic outputs or generated/edited 3D content.

Figure 3 overviews the pipeline. Section 3.1 describes how we extend a 2D VLM to operate 3D latents via a lightweight projector while keeping the VLM frozen. Section 3.2 details the 3D generation module, where learnable queries extract knowledge from the VLM and a transformer connector aligns these representations to the conditional space of a pretrained 3D diffusion model. Section 3.3 shows how the same mechanism supports instruction-driven 3D editing conditioned on an input shape. Finally, Section 3.4 outlines data curation.

3.1 3D Understanding

We extend a 2D VLM to the 3D domain to model $p_\theta(t | x)$, where x is a 3D shape and t is text. We use QwenVL-2.5 [12] as the base VLM Φ and encode x with the Hunyuan3D 2.1

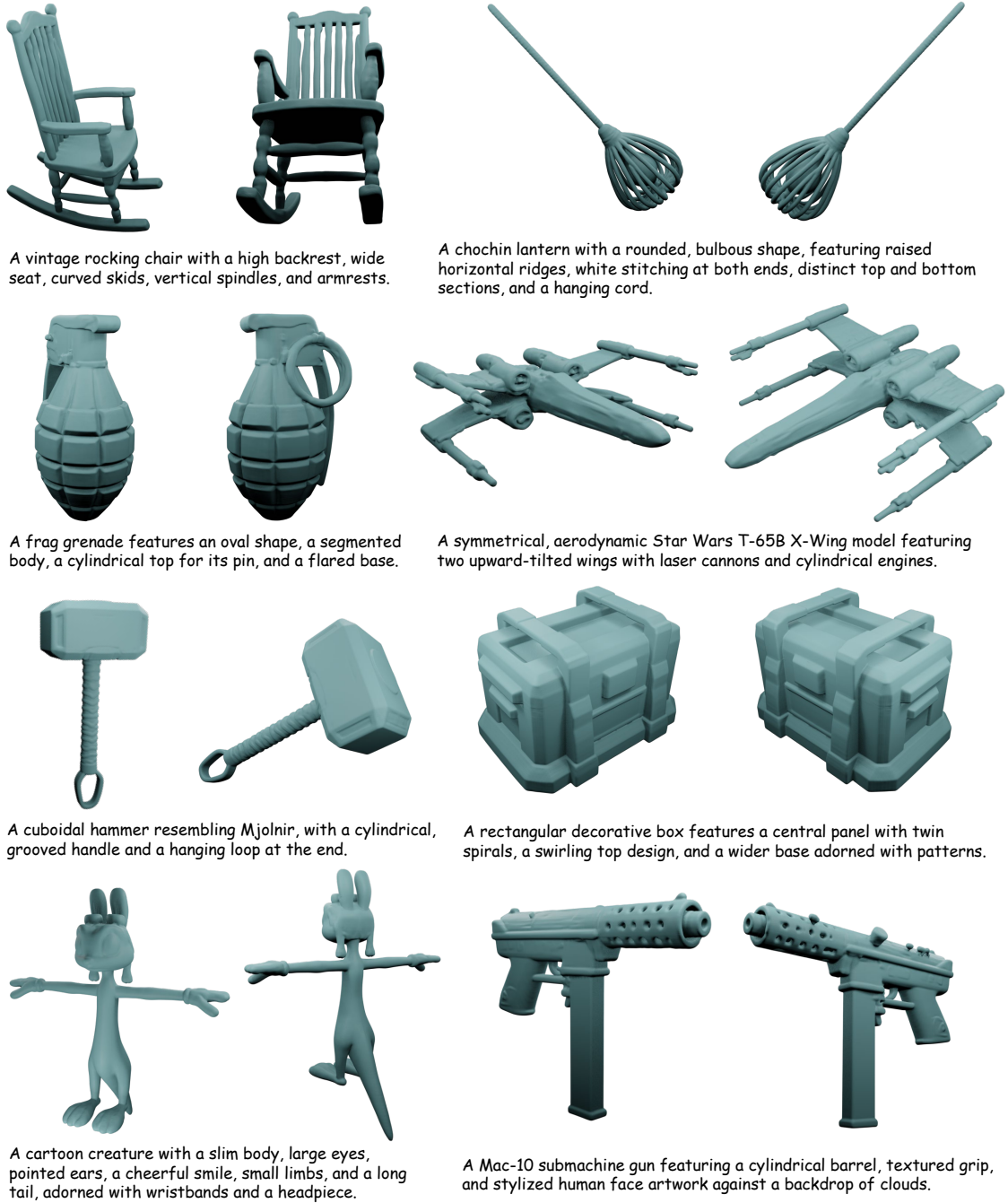


Fig. 2: Qualitative text-to-3D generation results. PNP-U3D is capable of generating diverse and high-quality 3D models.

VAE [36] denoted Ω , yielding a sequence of continuous 3D latents $u = \Omega(x)$. To interface with Φ , we introduce a lightweight MLP projector φ (four fully connected layers) that maps u to the VLM’s

token embedding space. Training follows standard autoregressive next-token prediction with cross-entropy:

$$\hat{t} = \Phi(\varphi(\Omega(x))), \quad \mathcal{L}_{\text{und}} = \text{CE}(\hat{t}, t_{\text{gt}}), \quad (1)$$

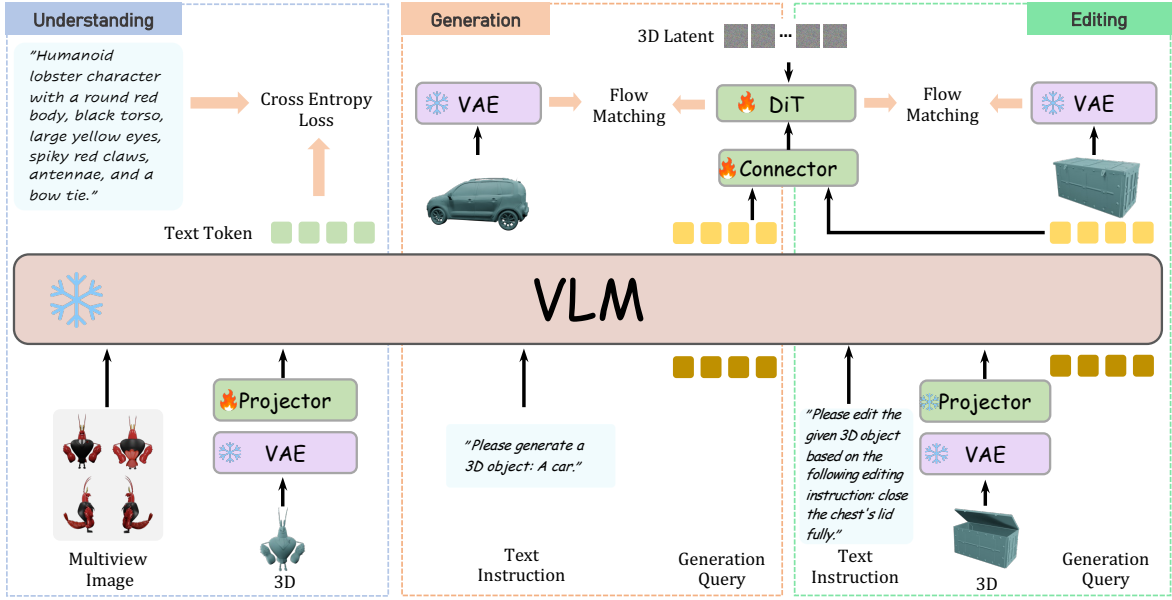


Fig. 3: Framework overview. PnP-U3D uses an autoregressive next-token paradigm for understanding and a continuous diffusion paradigm for generation. The two components interact via a trainable cross-modal connector.

where \hat{t} denotes the predicted token distribution and t_{gt} the ground-truth text. We freeze Φ (and Ω) and train only φ . This preserves the VLM’s general multimodal priors while enabling 3D understanding.

At inference, users may optionally provide multi-view images to supply texture cues missing from the 3D latents. These images are processed by the VLM’s vision tower. We use the following prompt template: “Given *<ThreeD>* the 3D representation and *<image>* multi-view images of the object (front, back, left, right), provide a detailed description of the object.”

3.2 3D Generation

We next describe the text-to-3D generation pipeline, which approximates the conditional distribution $p_\theta(x \mid t)$, where t is a user-provided textual instruction and x is the generated 3D shape. Inspired by [2, 4], given input text t , we concatenate a fixed-length set of learnable queries Q after t to form the sequence $[t; Q]$. Passing it through the VLM Φ yields enriched high-level features in which the queries capture domain knowledge and context from the pretrained model.

These query features serve as a cross-modal bridge to the 3D generation module.

To align the query features with the conditional input space of the pretrained 3D diffusion model, we employ a transformer connector ω . This connector maps the sequence $\Phi([t; Q])$ into the conditioning space expected by the diffusion transformer DiT, which is pretrained for image-conditioned 3D generation. The forward process is:

$$z = \text{DiT}(\omega(\Phi([t; Q])), \epsilon), \quad \mathcal{L}_{\text{gen}} = \text{FM}(\Omega(x_{\text{gt}}), z), \quad (2)$$

where z is the generated 3D latent, ϵ is Gaussian noise, $\Omega(x_{\text{gt}})$ is the ground-truth latent encoding of the target 3D shape, and FM denotes the flow-matching loss [35, 65, 66]. By supervising with \mathcal{L}_{gen} , the model learns to align the diffusion outputs with the ground-truth latent codes. During training, we freeze the VLM Φ and optimize the queries Q , connector ω , and diffusion backbone DiT. This ensures efficient training while leveraging powerful pretrained priors for both language and 3D generation.

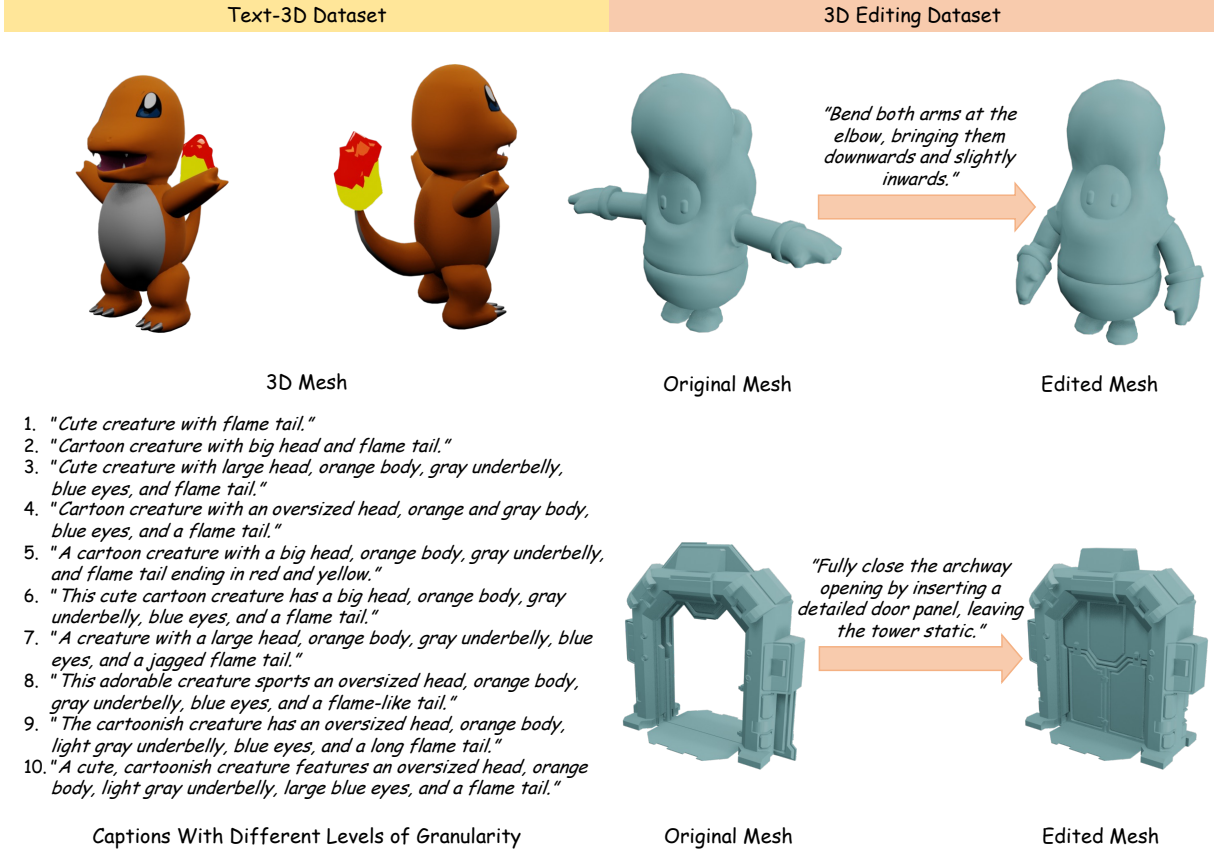


Fig. 4: Illustration of our *Text-3D* and *3D Editing Datasets*. The *Text-3D Dataset* pairing 3D shapes with multi-granular textual descriptions for 3D understanding and generation, and the *3D Editing Dataset* pairing edited 3D shapes with editing prompts for instruction-driven editing.

3.3 3D Editing

Finally, we extend the framework to instruction-guided 3D editing. The objective is to approximate $p_\theta(x_{\text{edit}} | x_{\text{input}}, t)$, where x_{input} is an input 3D shape, t is a textual instruction, and x_{edit} is the resulting edited shape.

We begin by encoding x_{input} into a latent $\Omega(x_{\text{input}})$. This latent, together with the text t and learnable queries Q , forms the combined sequence $[t; \Omega(x_{\text{input}}); Q]$. This sequence is processed by the VLM Φ to extract features that jointly encode both the 3D structure of the input and the textual guidance. The connector ω maps these features to the conditional space of the pretrained 3D diffusion model DiT, which then produces an edited latent z_{edit} :

$$\begin{aligned} z_{\text{edit}} &= \text{DiT}(\omega(\Phi([t; \Omega(x_{\text{input}}); Q])), \epsilon), \\ \mathcal{L}_{\text{edit}} &= \text{FM}(\Omega(x_{\text{edit}}), z_{\text{edit}}). \end{aligned} \quad (3)$$

Here $\mathcal{L}_{\text{edit}}$ supervises the alignment of the predicted edited latent with the ground-truth edited latent $\Omega(x_{\text{edit}})$. This setup leverages the VLM's understanding capability to condition generation on both shape and text, producing edits that respect the geometry of the original while reflecting the instruction.

3.4 Dataset

We curate two datasets: a *Text-3D* dataset pairing shapes with multi-granularity textual descriptions for understanding and generation, and a *3D Editing* dataset pairing edited shapes with prompts.

Text-3D Dataset. For each 3D mesh, we render four canonical views (front, back, left, right) under fixed camera intrinsics and arrange them into a 2×2 multi-view grid. This grid is

provided to GPT-4o to produce multi-granularity 3D captions. Each caption set covers: (i) semantic category, (ii) geometric structure (global shape and part-level attributes), (iii) texture-/material appearance, and (iv) function and style descriptors. We perform quality control via self-consistency checks across granularities and remove near-duplicate or low-content captions. To expose the model to varying levels of user specificity, we provide 10 annotation levels ranging from concise to detailed, with examples in Fig. 4.

3D Editing Dataset. To preserve 3D consistency in edit pairs, we leverage 4D sequences (animated objects) and treat different frames as pre-/post-edit states. Starting from a filtered list of 4D objects [67], we render four canonical views (front, back, left, right) of both the first and the 24th frames. The four views of each frame are concatenated into a 2×2 grid, yielding an image pair per object. We prompt a vision–language model (Gemini [68]) to (a) retain only pairs that exhibit a salient object-centric change (excluding camera/lighting changes), and (b) generate a concise editing instruction describing the transformation. For data augmentation, we request two instructions per retained pair: one for the forward change (frame 1 \rightarrow frame 24) and one for the reverse (frame 24 \rightarrow frame 1). This procedure yields over 14K 3D shape-editing-prompt pairs. The detailed instruction template used in the API call is provided as follows:

```
Act as a meticulous 3D technical
artist. Your task is to analyze two
multi-view composite images ('before'
and 'after'). Each image is stitched
together from four perspectives (front
, back, left, and right) to show the
entire 3D object.

Based on your analysis, generate a
single, descriptive instruction that
accurately explains the transformation
.

Your instruction must follow two
strict rules:
1. No Numbers: Do not use any numbers
, percentages, degrees, or other
quantitative measurements. Use
descriptive words to convey scale and
magnitude (e.g., 'slightly', 'sharply'
, 'fully', 'gently').
```

2. Be Concise: The entire instruction must be under 30 words.

The instruction should still clearly identify the component and the action (e.g., bend, stretch, twist, inflate, rotate).

Good Example Instructions:

- "Significantly stretch both legs outwards while maintaining their original thickness."

If there is no discernible difference between the images, respond with the exact string: 'error'. Do not provide any other explanation.

4 Experiments

4.1 Implementation Details

For the Text-3D dataset, we curate a high-quality corpus from G-Objaverse [69], where each object is annotated with 10 levels of captions ranging from concise to detailed, resulting in over 320K objects with 10 captions each. For the 3D editing dataset, we filter Diffusion4D [67] and obtain more than 14K shape-prompt pairs. For 3D understanding, we adopt a high-quality subset of 40K shapes. Our training pipeline consists of three stages: 3D understanding, text-to-3D generation, and instruction-guided 3D editing. Each stage is trained with its own dataset, optimization objective, and module-freezing strategy, as described below.

3D Understanding. In the first stage, we train a lightweight MLP that maps 3D latent representations into the token embedding space of a pretrained vision–language model. The input 3D shape is first encoded by the pretrained Hunyuan 2.1 3D autoencoder [36] into a latent token sequence, while the Qwen 2.5 vision–language backbone [12] remains frozen. Only the projection MLP is optimized using an autoregressive next-token prediction loss. This stage is trained on a high-quality subset of our Text-3D dataset containing 40K shapes, each paired with 10 textual descriptions. Training is run for 60K steps with a total batch size of 128 on 4 GPUs, using a learning rate of 10^{-4} . All pretrained components remain frozen to preserve their prior knowledge.

Text-to-3D Generation. The second stage learns to align the high-level representations produced by the vision-language model [12] with the conditional input space of a pretrained 3D diffusion model. Given a text prompt with 64 learnable queries, the frozen language model produces a sequence of semantic features, which are transformed by a trainable connector into the embedding space required by the diffusion backbone. The model is optimized using a flow-matching objective over the 3D latent codes encoded by the pretrained 3D autoencoder [36]. This stage is trained on 320K objects from our Text-3D dataset for 280K steps using a total batch size of 672 on 24 GPUs, with an optimizer configured with a learning rate of 10^{-4} and a latent size of 1024. The language model remains frozen, while the connector and diffusion backbone are fully trainable.

3D Editing. The final stage extends the same autoregressive-diffusion architecture to edit an input shape according to a provided textual instruction. The input consists of the instruction text, the latent representation of the source shape, and 1024 learnable query tokens that facilitate fine-grained control. The frozen language model extracts joint text-shape features, which the connector maps into the diffusion model’s conditional space. The edited 3D latent is supervised using a flow-matching objective against target edit examples. Training uses our 3D-Editing dataset, which includes 14K instruction-shape pairs, and is run for 80K steps with a total batch size of 112 on 8 GPUs. Pretrained modules remain frozen while the connector and diffusion backbone are updated.

Checkpointing and Model Selection. Models are selected using the final training checkpoint at the completion of the target training steps, rather than intermediate checkpoints based on validation performance. During text-to-3D inference, we optionally increase the latent resolution from 1024 to 4096 to obtain higher geometric fidelity without retraining.

4.2 Quantitative and Qualitative Comparisons

3D Understanding. We annotated a high-quality set of 917 detailed object captions on the Objaverse dataset [70] using GPT-4o to serve as ground truth for evaluating different methods.

Table 1 and Fig. 5 present both quantitative and qualitative comparisons between our approach and other state-of-the-art methods on the 3D object captioning task. As noted in PointLLM [6], BLEU-1, ROUGE-L, and METEOR tend to favor short captions and are limited in capturing semantic accuracy and diversity. We therefore place greater emphasis on Sentence-BERT and SimCSE scores. It is evident that when relying solely on 3D latents, our method may suffer from hallucinations regarding color and other texture-related attributes due to the lack of explicit texture information. Nevertheless, our approach still outperforms ShapeLLM-Omni [11]. Fig. 5 shows that PointLLM [6] tends to produce verbose descriptions with invalid information and hallucinations. Furthermore, by incorporating multi-view 2D images to provide complementary texture cues, our method achieves the best overall performance. This also highlights the strong scalability and flexibility of our framework. We additionally report the performance of our base model QwenVL-2.5 on multi-view images in Table 1 to further demonstrate the superiority of our approach.

3D Generation. We evaluate our method on the text-to-3D generation task. Qualitative results are presented in Fig. 2, showing that by incorporating a Transformer-based connector, our approach effectively maps the conditional space from images to high-level text, enabling the generation of detailed 3D shapes that align well with user prompts. This demonstrates the effectiveness of our design. For quantitative evaluation, we use Gemini [68] to generate 643 text prompts and compare against four representative text-to-3D baselines: Trellis [8], ShapeLLM-Omni [11], SAR3D [33], and GaussianAnything [23]. Each generated object is rendered into 24 views for evaluation. We report CLIP-score [72] with ViT-L/14 and RN50 \times 4 backbones, Q-Align [73] to assess alignment between generated assets and text prompts, and MUSIQ-AVA [74] to measure aesthetic quality. As shown in Table 2, our method achieves the best Q-Align score, indicating superior text-shape alignment. While Trellis slightly outperforms us on CLIP and MUSIQ-AVA scores, our method still surpasses ShapeLLM-Omni, SAR3D, and GaussianAnything by a clear margin. More importantly, unlike these baselines which are either trained from scratch or fine-tuned from text-to-3D models, our pipeline is

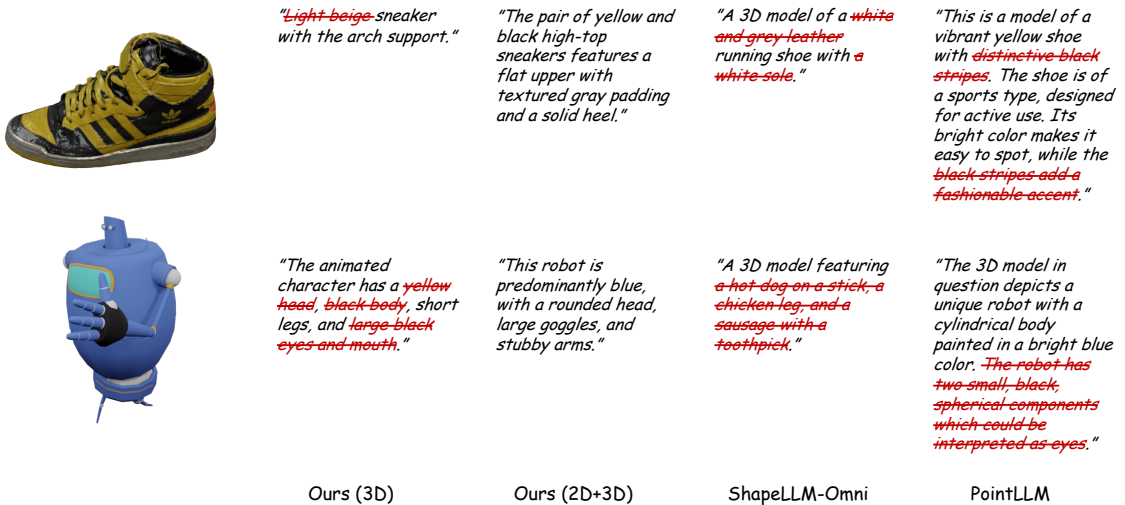


Fig. 5: Qualitative comparison on 3D object captioning. Benefiting from the flexibility of our framework, combining additional 2D information with the 3D latent yields more accurate and detailed captions. In contrast, PointLLM [6] often generates overly long outputs with meaningless redundancy and still suffers from hallucination issues. Note that our method may produce hallucinations due to the lack of texture information in the 3D latent.

Table 1: 3D object captioning results on Objaverse [70, 71]. Following PointLLM [6], we note that BLEU-1, ROUGE-L, and METEOR often favor short captions and insufficiently reflect semantic accuracy or diversity. Accordingly, we highlight Sentence-BERT and SimCSE scores as more reliable metrics.

Method	BLEU-1	ROUGE-L	METEOR	Sentence-BERT	SimCSE
PointLLM-7B [6]	8.70	11.07	13.25	55.76	58.27
PointLLM-13B [6]	8.53	11.00	13.08	55.50	57.96
ShapeLLM-Omni [11]	<u>13.55</u>	<u>16.44</u>	10.50	35.71	38.66
QwenVL-2.5 (2D)	8.04	8.33	6.27	42.75	47.93
Ours (3D)	12.86	15.38	10.26	45.80	47.42
Ours (2D+3D)	19.75	19.97	16.41	61.03	64.80

initialized from an image-conditioned model and is further extensible to 3D understanding and editing tasks beyond pure text-to-3D generation. Beyond quantitative results, Fig. 6 highlights that our model can capture fine-grained details explicitly described in the prompt but often ignored by other methods. For example, given the instruction ‘‘circular cut-outs’’, our model faithfully generates the circular cut-out, whereas competing approaches miss this detail. This suggests that the query extracted from the VLM prior enables our model to attend more closely to subtle textual cues, even if such improvements are not fully reflected in standard metrics. In addition, we compare with the base image-conditioned model Hunyuan 2.1 [36]. Specifically, we first generate an

image using the input prompt with Flux [75], and then feed the image into Hunyuan 2.1. As shown in Fig. 6, our lightweight design is able to preserve the strong generative ability of the base model while incorporating strong text alignment, thus achieving both high-quality geometry and faithful adherence to user prompts. Our more text-to-3D visual results are shown in Fig. 7.

3D Editing. We further demonstrate the capability of our pipeline on 3D editing. As shown in Fig. 8, the user can provide a 3D shape together with a natural language editing prompt, and our model modifies the overall geometry accordingly. Unlike traditional approaches that require users to manually specify local regions to be edited, our design directly interprets the prompt



Fig. 6: Qualitative comparison on 3D generation. Compared with competing methods, our approach generates high-quality 3D shapes, capturing fine-grained details while aligning well with user input, and meanwhile preserves the generative ability of the base image-conditioned model. * indicates the image-conditioned base model used.

Table 2: Quantitative comparison on text-to-3D generation. We report CLIP-score [72] (ViT-L/14 and RN50 \times 4), Q-Align [73], and MUSIQ-AVA [74] across four representative baselines and our method. Our approach achieves the best Q-Align score, indicating superior text–shape alignment, while maintaining competitive performance on CLIP and MUSIQ-AVA.

Method	ViT-L/14 \uparrow	RN50 \times 4 \uparrow	MUSIQ-AVA \uparrow	Q-Align \uparrow
Trellis [8]	27.91	42.75	5.20	2.11
Shape-Omni [11]	25.63	40.74	5.05	1.81
SAR3D [33]	25.88	40.80	4.90	1.79
GA [23]	24.91	38.71	4.62	1.56
Ours	<u>27.54</u>	<u>42.19</u>	<u>5.07</u>	2.12

and 3D shape latent at the semantic level. For example, when asked to “extending the left arm outwards,” our model automatically identifies the relevant limbs and performs consistent articulations, while preserving the identity and style of the original shape. To achieve this, we set a longer

query length (1024) to capture more fine-grained part-level semantics from the input mesh, which enables the model to better maintain shape identity during editing. Users only need to describe the desired modification in natural language, while the model automatically infers the spatial regions



A low-top sneaker featuring a rounded toe, geometric patterns, laces, and a sole with a slightly elevated heel.



An hourglass-shaped waist trainer with vertical seams and adjustable hooks.



A minimalist bench with a horizontal slatted seating surface, curved legs, and scroll armrests.



A helmet with a crest, a rounded dome shape, and ear cut-outs, inspired by Roman or Spartan styles.



A medieval key with a diamond-shaped head, an elongated cylindrical shaft, and a pointed two-pronged bit.



A KA-BAR knife with a sleek, long blade, a cylindrical grip featuring rings, a guard, and a pommel.

Fig. 7: More text-to-3D visual results. PnP-U3D is capable of generating diverse and high-quality 3D models.

to be edited. Moreover, our method demonstrates the ability to handle prompts that are out of distribution. For instance, as shown in the second example, our model successfully transforms the male figure into a female figure with longer

hair, while preserving the original hat, boots, and standing pose. This type of appearance modification lies outside the distribution of our dataset, which predominantly focuses on pose variations and shape deformations.

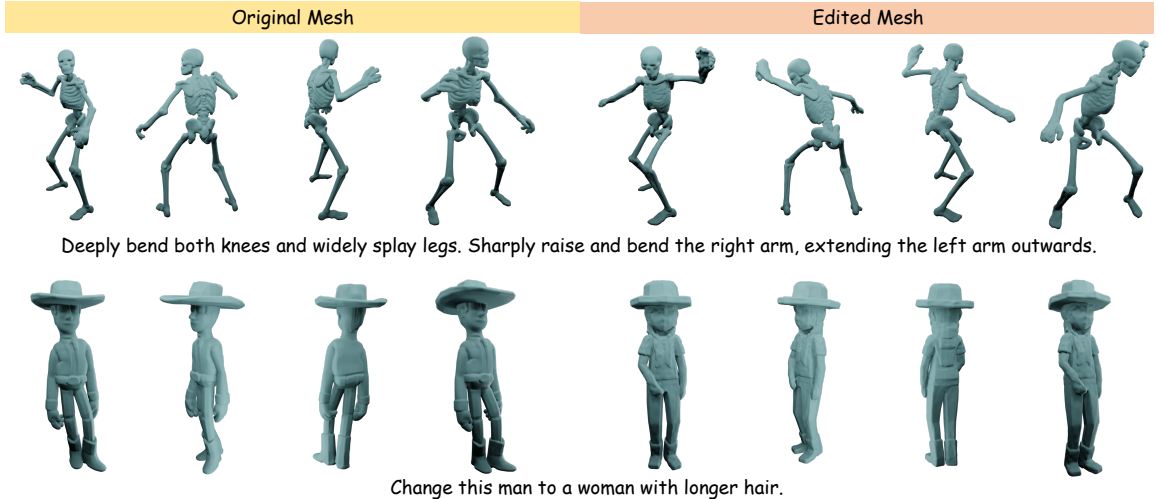


Fig. 8: Qualitative results on 3D editing. Our method edits input meshes according to natural language prompts, achieving diverse pose and appearance changes while preserving identity-related attributes, and it also works for out-of-distribution edits.

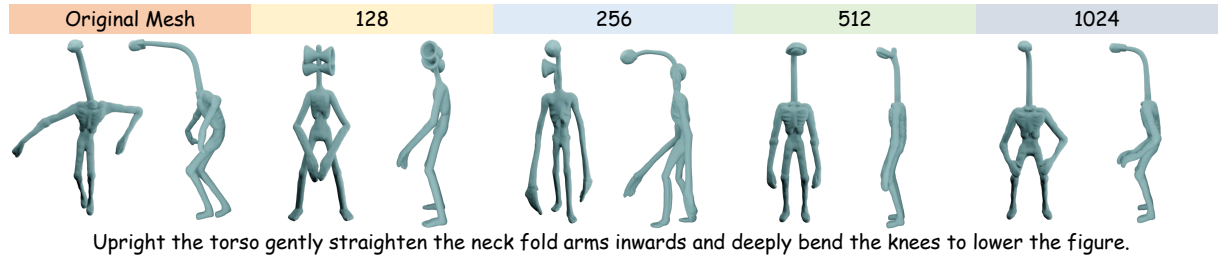


Fig. 9: Ablation on query length for 3D editing. Editing results with different query token lengths (128–1024). Longer queries alleviate the information bottleneck and better preserve the original attributes of the input mesh while performing the requested edits.

4.3 Ablation Study

Different Query Length for 3D Editing. In our editing experiments, we observe that the number of query tokens required by the generation module plays a crucial role in preserving the fidelity of the input 3D object. Fig. 9 illustrates the editing results with token lengths ranging from 128 to 1024. It is evident that longer query tokens effectively alleviate the information bottleneck, thereby better retaining the original attributes of the input 3D object. Moreover, as the token length increases, the edited object’s pose aligns more closely with the textual instruction, while the overall shape identity of the input mesh is also better preserved. These results highlight that increasing the token length consistently

improves both semantic alignment and geometric consistency in 3D editing.

Robust and Lightweight Training Strategy. Although our 3D generative model is trained only on 3D latents of length 1024, it generalizes effectively to longer token lengths (2048 and 4096) at inference, producing more fine-grained and detailed 3D shapes (Fig. 10). This highlights not only the strong prior knowledge preserved from the base model [36] and the compatibility of our framework, but also the efficiency of our training strategy—requiring low training cost while supporting high-quality generation with extended latents.

Adaptation to Different 3D Generative Model. To verify the compatibility of our framework with different 3D generation models, we

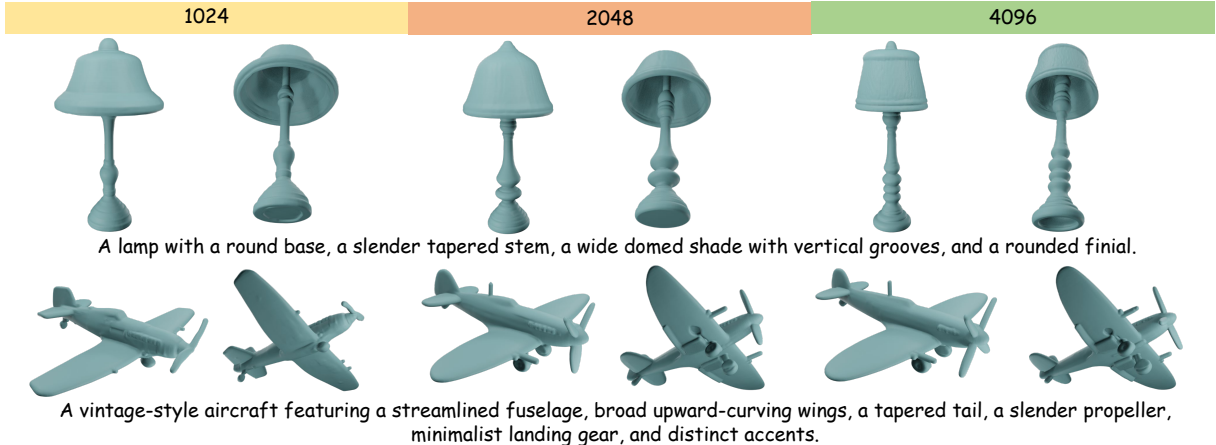


Fig. 10: Generalization to longer latents. Our model is trained with 1024 tokens but supports longer latents at inference, yielding finer 3D details with low training cost.

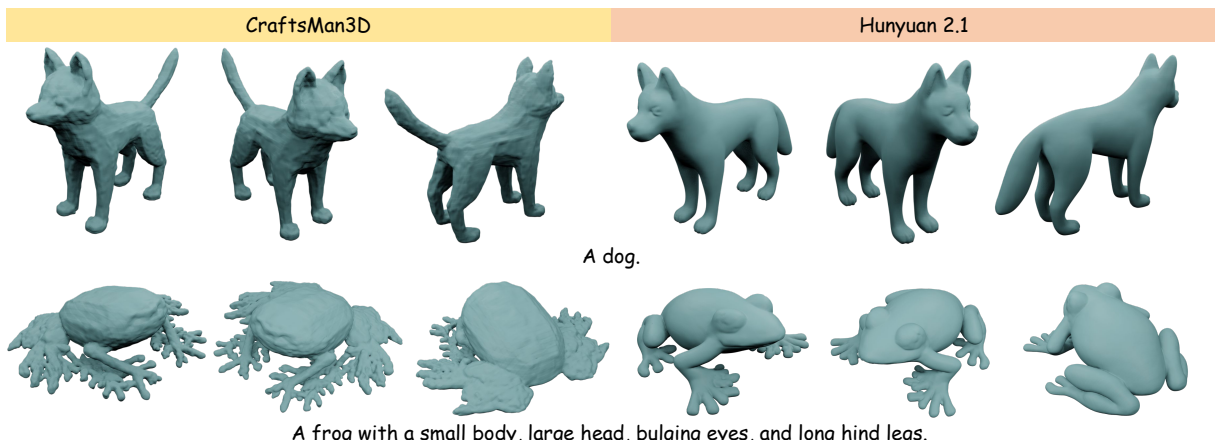


Fig. 11: Adaptation to different 3D generative models. Our framework works with different base models, demonstrating strong compatibility and producing 3D shapes faithful to text prompts.

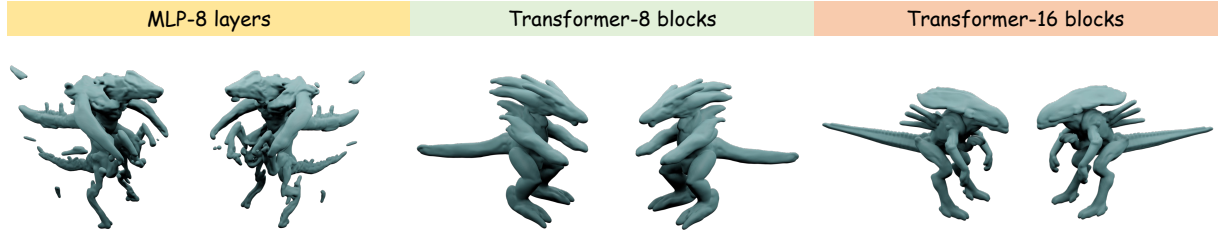
replace the generation base model with CraftsMan3D [76] while keeping all other settings unchanged. We train both models on 10K objects for 40K steps with a batch size of 56. As shown in Figure 11, our framework achieves text-to-3D synthesis with low training cost, demonstrating its lightweight and highly compatible nature.

Different Connector Designs. To study the effect of connector architecture and model capacity, we evaluate several connector designs, as illustrated in Figure 12. Specifically, we consider an 8-layer MLP, an 8-block Transformer, and a 16-block Transformer. As shown by the experimental results, Transformer-based connectors achieve better alignment between the latent spaces of

the generative model and the LLM. Moreover, increasing the depth of the Transformer further enhances its ability to transfer features extracted from the LLM to the generative model, leading to higher-quality generation results.

5 Conclusions

In this work, we presented the first unified framework integrating autoregression for 3D understanding with diffusion for 3D generation. By disentangling the paradigms of understanding and generation while enabling effective information exchange through a lightweight transformer, our approach preserves the strengths of standalone



A sleek, elongated Alien-queen features a large angular head, segmented tail, strong limbs with sharp claws

Fig. 12: Ablation results of different connector designs. We compare connectors with varying architectures and model capacities, including an 8-layer MLP, an 8-block Transformer, and a 16-block Transformer.

models and achieves state-of-the-art results across diverse 3D tasks. Moreover, we demonstrated strong potential in 3D editing, highlighting flexibility and extensibility. We believe our work sheds new light on the development of unified 3D understanding-generation models and intelligent 3D editing models, and hope it will further inspire the community to explore better architectures, training paradigms, and frameworks for advancing unified 3D intelligence.

References

- [1] Hurst, A., Lerer, A., Goucher, A.P., Perelman, A., Ramesh, A., Clark, A., Ostrow, A., Welihinda, A., Hayes, A., Radford, A., et al.: Gpt-4o system card. arXiv preprint arXiv:2410.21276 (2024)
- [2] Chen, J., Xu, Z., Pan, X., Hu, Y., Qin, C., Goldstein, T., Huang, L., Zhou, T., Xie, S., Savarese, S., et al.: Blip3-o: A family of fully open unified multimodal models—architecture, training and dataset. arXiv preprint arXiv:2505.09568 (2025)
- [3] Deng, C., Zhu, D., Li, K., Gou, C., Li, F., Wang, Z., Zhong, S., Yu, W., Nie, X., Song, Z., et al.: Emerging properties in unified multimodal pretraining. arXiv preprint arXiv:2505.14683 (2025)
- [4] Pan, X., Shukla, S.N., Singh, A., Zhao, Z., Mishra, S.K., Wang, J., Xu, Z., Chen, J., Li, K., Juefei-Xu, F., et al.: Transfer between modalities with metaqueries. arXiv preprint arXiv:2504.06256 (2025)
- [5] Ma, C., Jiang, Y., Wu, J., Yang, J., Yu, X., Yuan, Z., Peng, B., Qi, X.: Unitok: A unified tokenizer for visual generation and understanding. arXiv preprint arXiv:2502.20321 (2025)
- [6] Xu, R., Wang, X., Wang, T., Chen, Y., Pang, J., Lin, D.: Pointllm: Empowering large language models to understand point clouds. In: European Conference on Computer Vision, pp. 131–147 (2024). Springer
- [7] Zhang, B., Tang, J., Niessner, M., Wonka, P.: 3dshape2vecset: A 3d shape representation for neural fields and generative diffusion models. ACM Transactions on Graphics (TOG) **42**(4), 1–16 (2023)
- [8] Xiang, J., Lv, Z., Xu, S., Deng, Y., Wang, R., Zhang, B., Chen, D., Tong, X., Yang, J.: Structured 3d latents for scalable and versatile 3d generation. In: Proceedings of the IEEE/CVF Conference on Computer Vision and Pattern Recognition (CVPR), pp. 21469–21480 (2025)
- [9] Zhang, L., Wang, Z., Zhang, Q., Qiu, Q., Pang, A., Jiang, H., Yang, W., Xu, L., Yu, J.: Clay: A controllable large-scale generative model for creating high-quality 3d assets. ACM Transactions on Graphics (TOG) **43**(4), 1–20 (2024)
- [10] Lei, B., Li, Y., Liu, X., Yang, S., Xu, L., Huang, J., Tang, R., Weng, H., Liu, J., Xu, J., et al.: Hunyuan3d studio: End-to-end ai pipeline for game-ready 3d asset generation. arXiv preprint arXiv:2509.12815 (2025)

[11] Ye, J., Wang, Z., Zhao, R., Xie, S., Zhu, J.: Shapellm-omni: A native multimodal llm for 3d generation and understanding. Advances in Neural Information Processing Systems (2025)

[12] Bai, S., Chen, K., Liu, X., Wang, J., Ge, W., Song, S., Dang, K., Wang, P., Wang, S., Tang, J., et al.: Qwen2. 5-vl technical report. arXiv preprint arXiv:2502.13923 (2025)

[13] Song, Y., Sohl-Dickstein, J., Kingma, D.P., Kumar, A., Ermon, S., Poole, B.: Score-based generative modeling through stochastic differential equations. In: International Conference on Learning Representations (ICLR) (2021)

[14] Ho, J., Jain, A., Abbeel, P.: Denoising diffusion probabilistic models. Advances in Neural Information Processing Systems (NeurIPS) (2020)

[15] Esser, P., Rombach, R., Ommer, B.: Tampering transformers for high-resolution image synthesis. In: Proceedings of the IEEE/CVF Conference on Computer Vision and Pattern Recognition (CVPR), pp. 12873–12883 (2021)

[16] Han, J., Wang, J., Vedaldi, A., Torr, P., Kokkinos, F.: Flex3d: Feed-forward 3d generation with flexible reconstruction model and input view curation. arXiv preprint arXiv:2410.00890 (2024)

[17] Poole, B., Jain, A., Barron, J.T., Mildenhall, B.: Dreamfusion: Text-to-3d using 2d diffusion. In: International Conference on Learning Representations (ICLR) (2023)

[18] Wang, Z., Lu, C., Wang, Y., Bao, F., Li, C., Su, H., Zhu, J.: Prolificdreamer: High-fidelity and diverse text-to-3d generation with variational score distillation. In: Advances in Neural Information Processing Systems (NeurIPS) (2023)

[19] Chen, R., Chen, Y., Jiao, N., Jia, K.: Fantasia3d: Disentangling geometry and appearance for high-quality text-to-3d content creation. In: Proceedings of the IEEE/CVF International Conference on Computer Vision (ICCV), pp. 22246–22256 (2023)

[20] Vahdat, A., Williams, F., Gojcic, Z., Litany, O., Fidler, S., Kreis, K., et al.: Lion: Latent point diffusion models for 3d shape generation. Advances in Neural Information Processing Systems (NeurIPS) **35**, 10021–10039 (2022)

[21] Lan, Y., Hong, F., Yang, S., Zhou, S., Meng, X., Dai, B., Pan, X., Loy, C.C.: Ln3diff: Scalable latent neural fields diffusion for speedy 3d generation. In: Proceedings of the European Conference on Computer Vision (ECCV), pp. 112–130 (2024). Springer

[22] Li, W., Liu, J., Yan, H., Chen, R., Liang, Y., Chen, X., Tan, P., Long, X.: Crafts-Man: High-fidelity mesh generation with 3D native generation and interactive geometry refiner. In: Proceedings of the IEEE/CVF Conference on Computer Vision and Pattern Recognition (CVPR) (2025)

[23] Lan, Y., Zhou, S., Lyu, Z., Hong, F., Yang, S., Dai, B., Pan, X., Loy, C.C.: Gaussiananything: Interactive point cloud latent diffusion for 3d generation. In: International Conference on Learning Representations (ICLR) (2025)

[24] Chen, Z., Tang, J., Dong, Y., Cao, Z., Hong, F., Lan, Y., Wang, T., Xie, H., Wu, T., Saito, S., Pan, L., Lin, D., Liu, Z.: 3dtopia-xl: High-quality 3d pbr asset generation via primitive diffusion. arXiv preprint arXiv:2409.12957 (2024)

[25] Di, D., Yang, J., Luo, C., Xue, Z., Chen, W., Yang, X., Gao, Y.: Hyper-3dg: Text-to-3d gaussian generation via hypergraph. International Journal of Computer Vision **133**(5), 2886–2909 (2025)

[26] Pan, Z., Yang, Z., Zhu, X., Zhang, L.: Efficient4d: Fast dynamic 3d object generation from a single-view video. International Journal of Computer Vision **134**(1), 14 (2026)

[27] Li, M., Zhou, P., Liu, J.-W., Keppo, J., Lin,

M., Yan, S., Xu, X.: Instant3d: Instant text-to-3d generation. *International Journal of Computer Vision* **132**(10), 4456–4472 (2024)

[28] Hu, S., Hong, F., Hu, T., Pan, L., Mei, H., Xiao, W., Yang, L., Liu, Z.: Humanliff: Layer-wise 3d human diffusion model. *International Journal of Computer Vision*, 1–20 (2025)

[29] Kingma, D.P., Welling, M.: Auto-encoding variational bayes. *arXiv* (2013)

[30] Tian, K., Jiang, Y., Yuan, Z., Peng, B., Wang, L.: Visual autoregressive modeling: Scalable image generation via next-scale prediction. *Advances in Neural Information Processing Systems (NeurIPS)* **37**, 84839–84865 (2024)

[31] Cho, I., Yoo, Y., Jeon, S., Kim, S.J.: Representing 3d shapes with 64 latent vectors for 3d diffusion models. In: *Proceedings of the IEEE/CVF International Conference on Computer Vision (ICCV)* (2025)

[32] Chen, R., Zhang, J., Liang, Y., Luo, G., Li, W., Liu, J., Li, X., Long, X., Feng, J., Tan, P.: Dora: Sampling and benchmarking for 3d shape variational auto-encoders. In: *Proceedings of the IEEE/CVF Conference on Computer Vision and Pattern Recognition (CVPR)*, pp. 16251–16261 (2025)

[33] Chen, Y., Lan, Y., Zhou, S., Wang, T., Pan, X.: Sar3d: Autoregressive 3d object generation and understanding via multi-scale 3d vqvae. In: *Proceedings of the IEEE/CVF Conference on Computer Vision and Pattern Recognition (CVPR)*, pp. 28371–28382 (2025)

[34] Peebles, W., Xie, S.: Scalable diffusion models with transformers. In: *Proceedings of the IEEE/CVF International Conference on Computer Vision (ICCV)*, pp. 4195–4205 (2023)

[35] Ma, N., Goldstein, M., Albergo, M.S., Boffi, N.M., Vanden-Eijnden, E., Xie, S.: Sit: Exploring flow and diffusion-based generative models with scalable interpolant transformers. In: *Proceedings of the European Conference on Computer Vision (ECCV)*, pp. 23–40 (2024). Springer

[36] Hunyuan3D, T., Yang, S., Yang, M., Feng, Y., Huang, X., Zhang, S., He, Z., Luo, D., Liu, H., Zhao, Y., et al.: Hunyuan3d 2.1: From images to high-fidelity 3d assets with production-ready pbr material. *arXiv preprint arXiv:2506.15442* (2025)

[37] Wu, S., Lin, Y., Zhang, F., Zeng, Y., Xu, J., Torr, P., Cao, X., Yao, Y.: Direct3D: Scalable image-to-3d generation via 3d latent diffusion transformer. In: *Advances in Neural Information Processing Systems (NeurIPS)* (2024)

[38] Achiam, J., Adler, S., Agarwal, S., Ahmad, L., Akkaya, I., Aleman, F.L., Almeida, D., Altenschmidt, J., Altman, S., Anadkat, S., et al.: Gpt-4 technical report. *arXiv preprint arXiv:2303.08774* (2023)

[39] Touvron, H., Lavril, T., Izacard, G., Martinet, X., Lachaux, M.-A., Lacroix, T., Rozière, B., Goyal, N., Hambro, E., Azhar, F., et al.: Llama: Open and efficient foundation language models. *arXiv preprint arXiv:2302.13971* (2023)

[40] Touvron, H., Martin, L., Stone, K., Albert, P., Almahairi, A., Babaei, Y., Bashlykov, N., Batra, S., Bhargava, P., Bhosale, S., et al.: Llama 2: Open foundation and fine-tuned chat models. *arXiv preprint arXiv:2307.09288* (2023)

[41] Yang, A., Li, A., Yang, B., Zhang, B., Hui, B., Zheng, B., Yu, B., Gao, C., Huang, C., Lv, C., et al.: Qwen3 technical report. *arXiv preprint arXiv:2505.09388* (2025)

[42] Li, W., Yuan, Y., Liu, J., Tang, D., Wang, S., Qin, J., Zhu, J., Zhang, L.: Tokenpacker: Efficient visual projector for multimodal llm. *International Journal of Computer Vision*, 1–19 (2025)

[43] Luo, T., Rockwell, C., Lee, H., Johnson, J.: Scalable 3d captioning with pretrained

models. *Advances in Neural Information Processing Systems (NeurIPS)* **36**, 75307–75337 (2023)

[44] Luo, T., Johnson, J., Lee, H.: View selection for 3d captioning via diffusion ranking. In: *Proceedings of the European Conference on Computer Vision (ECCV)*, pp. 180–197 (2024). Springer

[45] Zhou, J., Wang, J., Ma, B., Liu, Y.-S., Huang, T., Wang, X.: Uni3d: Exploring unified 3d representation at scale. In: *International Conference on Learning Representations (ICLR)* (2024)

[46] Hong, Y., Zhen, H., Chen, P., Zheng, S., Du, Y., Chen, Z., Gan, C.: 3d-llm: Injecting the 3d world into large language models. *Advances in Neural Information Processing Systems (NeurIPS)* **36**, 20482–20494 (2023)

[47] Hong, Y., Zhen, H., Chen, P., Zheng, S., Du, Y., Chen, Z., Gan, C.: 3d-llm: Injecting the 3d world into large language models. *Advances in Neural Information Processing Systems* **36**, 20482–20494 (2023)

[48] Qi, Z., Dong, R., Zhang, S., Geng, H., Han, C., Ge, Z., Yi, L., Ma, K.: Shapellm: Universal 3d object understanding for embodied interaction. In: *European Conference on Computer Vision*, pp. 214–238 (2024). Springer

[49] Zhou, Z., Wang, P., Liang, Z., Bai, H., Zhang, R.: Cross-modal 3d representation with multi-view images and point clouds. In: *Proceedings of the IEEE/CVF Conference on Computer Vision and Pattern Recognition (CVPR)*, pp. 3728–3739 (2025)

[50] Zuo, X., Samangouei, P., Zhou, Y., Di, Y., Li, M.: Fmgs: Foundation model embedded 3d gaussian splatting for holistic 3d scene understanding. *International Journal of Computer Vision* **133**(2), 611–627 (2025)

[51] Hamdi, A., AlZahrani, F., Giancola, S., Ghanem, B.: Mvtn: Learning multi-view transformations for 3d understanding. *International Journal of Computer Vision* **133**(4), 2197–2226 (2025)

[52] Liu, H., Yan, W., Zaharia, M., Abbeel, P.: World model on million-length video and language with blockwise ringattention. *arXiv preprint arXiv:2402.08268* (2024)

[53] Zhao, Y., Xue, F., Reed, S., Fan, L., Zhu, Y., Kautz, J., Yu, Z., Krähenbühl, P., Huang, D.-A.: Qlip: Text-aligned visual tokenization unifies auto-regressive multi-modal understanding and generation. *arXiv preprint arXiv:2502.05178* (2025)

[54] Lin, B., Li, Z., Cheng, X., Niu, Y., Ye, Y., He, X., Yuan, S., Yu, W., Wang, S., Ge, Y., et al.: Uniworld: High-resolution semantic encoders for unified visual understanding and generation. *arXiv preprint arXiv:2506.03147* (2025)

[55] Song, W., Wang, Y., Song, Z., Li, Y., Sun, H., Chen, W., Zhou, Z., Xu, J., Wang, J., Yu, K.: Dualtoken: Towards unifying visual understanding and generation with dual visual vocabularies. *arXiv preprint arXiv:2503.14324* (2025)

[56] Xie, J., Mao, W., Bai, Z., Zhang, D.J., Wang, W., Lin, K.Q., Gu, Y., Chen, Z., Yang, Z., Shou, M.Z.: Show-o: One single transformer to unify multimodal understanding and generation. *arXiv preprint arXiv:2408.12528* (2024)

[57] Wu, C., Chen, X., Wu, Z., Ma, Y., Liu, X., Pan, Z., Liu, W., Xie, Z., Yu, X., Ruan, C., et al.: Janus: Decoupling visual encoding for unified multimodal understanding and generation. In: *Proceedings of the Computer Vision and Pattern Recognition Conference*, pp. 12966–12977 (2025)

[58] Zhuang, X., Xie, Y., Deng, Y., Yang, D., Liang, L., Ru, J., Yin, Y., Zou, Y.: Vargpt-v1. 1: Improve visual autoregressive large unified model via iterative instruction tuning and reinforcement learning. *arXiv preprint arXiv:2504.02949* (2025)

[59] Li, T., Lu, Q., Zhao, L., Li, H., Zhu, X., Qiao,

Y., Zhang, J., Shao, W.: Unifork: Exploring modality alignment for unified multi-modal understanding and generation. arXiv preprint arXiv:2506.17202 (2025)

[60] Wu, Y., Zhang, Z., Chen, J., Tang, H., Li, D., Fang, Y., Zhu, L., Xie, E., Yin, H., Yi, L., et al.: Vila-u: a unified foundation model integrating visual understanding and generation. arXiv preprint arXiv:2409.04429 (2024)

[61] Wu, J., Jiang, Y., Ma, C., Liu, Y., Zhao, H., Yuan, Z., Bai, S., Bai, X.: Liquid: Language models are scalable and unified multi-modal generators. arXiv preprint arXiv:2412.04332 (2024)

[62] Wang, X., Zhang, X., Luo, Z., Sun, Q., Cui, Y., Wang, J., Zhang, F., Wang, Y., Li, Z., Yu, Q., et al.: Emu3: Next-token prediction is all you need. arXiv preprint arXiv:2409.18869 (2024)

[63] Zhou, C., Yu, L., Babu, A., Tirumala, K., Yasunaga, M., Shamis, L., Kahn, J., Ma, X., Zettlemoyer, L., Levy, O.: Transfusion: Predict the next token and diffuse images with one multi-modal model. arXiv preprint arXiv:2408.11039 (2024)

[64] Zhuang, X., Xie, Y., Deng, Y., Liang, L., Ru, J., Yin, Y., Zou, Y.: Vargpt: Unified understanding and generation in a visual autoregressive multimodal large language model. arXiv preprint arXiv:2501.12327 (2025)

[65] Lipman, Y., Chen, R.T.Q., Ben-Hamu, H., Nickel, M., Le, M.: Flow matching for generative modeling. In: International Conference on Learning Representations (ICLR) (2023)

[66] Liu, X., Gong, C., Liu, Q.: Flow straight and fast: Learning to generate and transfer data with rectified flow. In: International Conference on Learning Representations (ICLR) (2023)

[67] Liang, H., Yin, Y., Xu, D., Liang, H., Wang, Z., Plataniotis, K.N., Zhao, Y., Wei, Y.: Diffusion4d: Fast spatial-temporal consistent 4d generation via video diffusion models. arXiv preprint arXiv:2405.16645 (2024)

[68] Team, G.: Gemini 2.5: Pushing the Frontier with Advanced Reasoning, Multimodality, Long Context, and Next Generation Agentic Capabilities (2025). <https://arxiv.org/abs/2507.06261>

[69] Qiu, L., Chen, G., Gu, X., Zuo, Q., Xu, M., Wu, Y., Yuan, W., Dong, Z., Bo, L., Han, X.: Richdreamer: A generalizable normal-depth diffusion model for detail richness in text-to-3d. In: Proceedings of the IEEE/CVF Conference on Computer Vision and Pattern Recognition (CVPR), pp. 9914–9925 (2024)

[70] Deitke, M., Schwenk, D., Salvador, J., Weihs, L., Michel, O., VanderBilt, E., Schmidt, L., Ehsani, K., Kembhavi, A., Farhadi, A.: Objaverse: A universe of annotated 3d objects. In: Proceedings of the IEEE/CVF Conference on Computer Vision and Pattern Recognition (CVPR), pp. 13142–13153 (2023)

[71] Deitke, M., Liu, R., Wallingford, M., Ngo, H., Michel, O., Kusupati, A., Fan, A., Laforte, C., Voleti, V., Gadre, S.Y., et al.: Objaverse-xl: A universe of 10m+ 3d objects. Advances in Neural Information Processing Systems **36**, 35799–35813 (2023)

[72] Radford, A., Kim, J.W., Hallacy, C., Ramesh, A., Goh, G., Agarwal, S., Sastry, G., Askell, A., Mishkin, P., Clark, J., et al.: Learning transferable visual models from natural language supervision. In: International Conference on Machine Learning (ICML), pp. 8748–8763 (2021). PMLR

[73] Wu, H., Zhang, Z., Zhang, W., Chen, C., Liao, L., Li, C., Gao, Y., Wang, A., Zhang, E., Sun, W., et al.: Q-align: Teaching lmms for visual scoring via discrete text-defined levels. arXiv preprint arXiv:2312.17090 (2023)

[74] Ke, J., Wang, Q., Wang, Y., Milanfar, P., Yang, F.: Musiq: Multi-scale image quality transformer. In: Proceedings of the IEEE/CVF International Conference on Computer Vision (ICCV), pp. 5148–5157 (2021)

[75] Labs, B.F.: Flux. <https://github.com/>

black-forest-labs/flux. Accessed: September 23, 2025 (2024)

[76] Li, W., Liu, J., Yan, H., Chen, R., Liang, Y., Chen, X., Tan, P., Long, X.: Craftsman3d: High-fidelity mesh generation with 3d native generation and interactive geometry refiner. arXiv preprint arXiv:2405.14979 (2024)